Author/s:
Owyong, TC;Subedi, P;Deng, J;Hinde, E;Paxman, JJ;White, JM;Chen, W;Heras, B;Wong, WWH;Hong, Y

Title:
A Molecular Chameleon for Mapping Subcellular Polarity in an Unfolded Proteome Environment

Date:
2020-06-15

Citation:
Owyong, T. C., Subedi, P., Deng, J., Hinde, E., Paxman, J. J., White, J. M., Chen, W., Heras, B., Wong, W. W. H. & Hong, Y. (2020). A Molecular Chameleon for Mapping Subcellular Polarity in an Unfolded Proteome Environment. Angewandte Chemie, 132 (25), pp.10215-10221. https://doi.org/10.1002/ange.201914263.

Title: A Molecular Chameleon for Mapping Subcellular Polarity of Unfolded Proteome Environment

Authors: Tze Cin Owyong; Pramod Subedi; Jieru Deng; Elizabeth Hinde; Jason J Paxman; Jonathan M White; Weisan Chen; Begona Heras; Wallace W H Wong; Yuning Hong, Ph.D.

To be cited as: 10.1002/ange.201914263

Link to VoR: https://doi.org/10.1002/ange.201914263

A Molecular Chameleon for Mapping Subcellular Polarity of Unfolded Proteome Environment

Tze Cin Owyong,[a,b] Pramod Subedi,[c] Jieru Deng,[c] Elizabeth Hinde,[d] Jason J. Paxman,[c] Jonathan M. White,[a] Weisan Chen,[c] Begoña Heras,[c] Wallace W. H. Wong,*[a] and Yuning Hong*[b]

Abstract: Environmental polarity is an important factor in driving biomolecular interactions to regulate cell function. In this work, a general method of using the fluorogenic probe NTPAN-MI was reported to quantify the subcellular polarity change in response to protein unfolding. NTPAN-MI fluorescence is selectively activated upon labeling unfolded proteins with exposed thiols to report on the extent of proteostasis. NTPAN-MI was used to reveal the collapse of the host proteome caused by influenza A virus infection. The emission profile of NTPAN-MI contains information of the local polarity of the unfolded proteome, which can be resolved through spectral phasor analysis. Under stress conditions that disrupt different checkpoints of protein quality control, distinct patterns of dielectric constant distribution in the cytoplasm can be observed. However, in the nucleus, the unfolded proteome was found to experience a more hydrophilic environment across all the stress conditions, indicating the central role of nucleus in the stress response process.

Introduction

Folding of polypeptide chains into the correct native structure is essential for proteins to be functional.[1] To maintain the proteome in the folded state, cells adopt a sophisticated quality control system, known as proteostasis, to constantly keep the balance of the synthesis, maturation and degradation of cellular proteins. This system is governed by a network of over 800 proteins in humans.[2-3] Environmental perturbations or aberrant proteins (mutations, translational errors, etc.) can impair the buffering capacity of proteostasis and result in a backlog of proteins that are either not fully folded or aggregated, the latter is a common feature associated with neurodegeneration, cancers and autoimmune diseases.[4]

[a] T. C. Owyong, Prof., J. M. White, Dr., W. W. H. Wong
ARC Centre of Excellence in Exciton Science, School of Chemistry, Bio21 Institute, The University of Melbourne, Parkville, VIC 3010 Australia
E-mail: wwhwong@unimelb.edu.au
[b] T. C. Owyong, Dr., Y. Hong
Department of Chemistry and Physics, La Trobe Institute for Molecular Science, La Trobe University, Melbourne, VIC 3086, Australia
E-mail: Y.Hong@latrobe.edu.au
[c] P. Subedi, J. Deng, Dr., J. J. Paxman, Prof., W. Chen, A/Prof B. Heras
Department of Biochemistry and Genetics, La Trobe Institute for Molecular Science, La Trobe University, Melbourne, VIC 3086, Australia
[d] Dr., E. Hinde
School of Physics, Department of Biochemistry and Molecular Biology, Bio21 Institute, The University of Melbourne, VIC 3010, Australia

Supporting information for this article is given via a link at the end of the document.

Recent research has shown the connection between misfolded proteins and the formation of membraneless compartments, such as stress granules, p-bodies, and nuclear bodies, suggesting the crucial role of these compartments in buffering proteostasis stress.[5-7] Although the exact mechanism remains elusive, the change in the intracellular environment is considered as an important factor driving the assembly of these dynamic membraneless condensates.[7,8] A phase separation process mediates the formation of these bodies where the polarity of the interior is distinct from the general environment in the cytoplasm and nucleus.[9] Moreover, the environment in soluble, disordered aggregates of misfolded proteins has also been reported to be distinct from those of the ordered, fibrillar structures.[10,11] Therefore, quantifying the change of environmental polarity could provide a better understanding of the stress response mechanisms in the cell as well as informing about the pathogenicity associated with diseases related to protein misfolding.

Herein, we develop a general strategy to quantify the polarity, in terms of dielectric constant (ε), of the local environment surrounding unfolded proteins in cells. Our approach is based on a unique environment-sensitive fluorogenic dye: the fluorescence is activated upon reaction with unfolded proteins and the emission profile can be decoded to retrieve quantitative information of the dielectric constant in the cells. We validate our strategy *in vitro* by using purified model proteins and in cells under stress conditions that promote protein unfolding. We further apply our strategy to quantify the change of polarity surrounding unfolded proteins in different intracellular compartments driven by the increase of unfolded protein load. Compared to our previously reported approaches to quantifying cytoplasmic unfolded proteins,[12,13] this multi-responsive probe serves as a "molecular chameleon" that holds unprecedented advantage for direct visualizing and quantifying unfolded proteins in both the cytoplasm and the nucleus, with sensitivity to *in situ* environmental polarity changes in different subcellular compartments arising from protein unfolding.

Results and Discussion

Probe Design Rationale

Our design rationale is to target unfolded proteins in cells using a cysteine (Cys)-reactive aggregation-induced emission (AIE) fluorophore. We have recently demonstrated the use of maleimide (MI) functionalized tetraphenylethene (TPE-MI, **1**, Figure 1A) for measuring the unfolded protein load as a proxy reporter of the proteostasis capacity inside the cells.[12] The activation of TPE-MI fluorescence has two criteria: the removal of the photoinduced electron transfer (PeT) quenching effect of MI and the restriction of the intramolecular motions of TPE. The MI

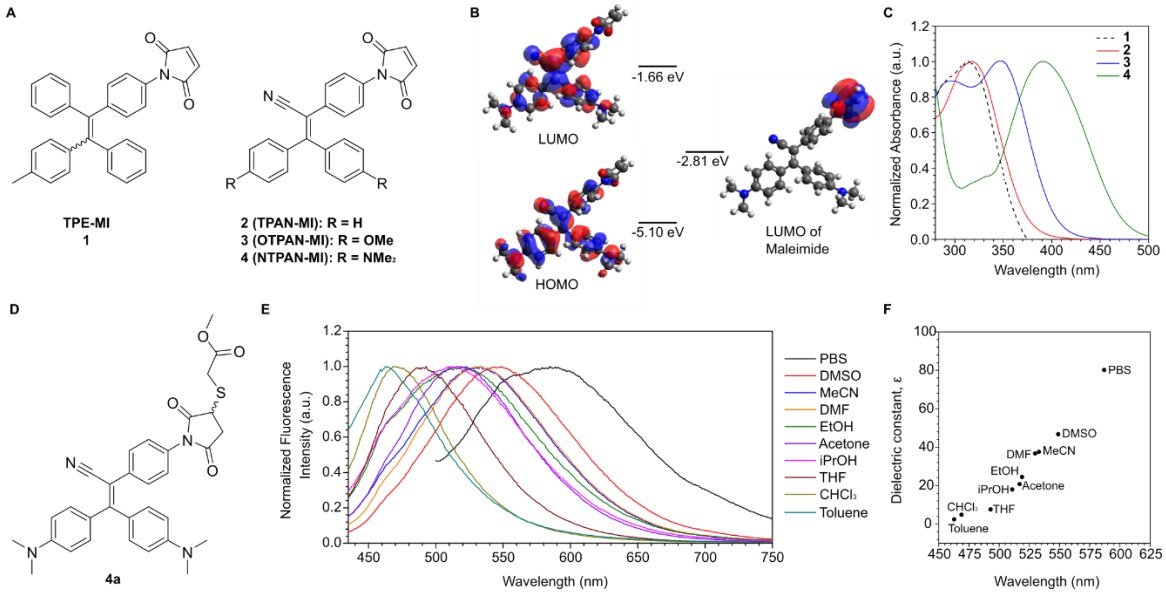

Figure 1. Dye structures and photophysical characterization. (A) Chemical structures of previously reported (**1**) and newly synthesized thiol-reactive probes (**2**-**4**). (B) HOMO and LUMO energy levels for **4** (NTPAN-MI). (C) Normalized UV-Vis absorbance spectra for compound **1**-**4** in DMSO. (D) Model thiol-conjugate NTPAN-MI (**4a**). (E) Normalized fluorescence spectra of **4a** in solvents with different polarity. (F) Correlation of the emission maximum of **4a** *versus* dielectric constant (ε) of solvents. Excitation wavelength: 405 nm. Dye concentration: 50 μM.

moiety enables the specific targeting on Cys residues in the free thiol form which are usually buried in folded proteins but become exposed when proteins unfold. Upon reacting with a Cys, the PeT effect can be suppressed. Meanwhile, the hydrophobic sidechains on unfolded proteins can provide an environment that contributes to TPE fluorescence. This unique property enables the differentiation of Cys residues on unfolded proteins from small biothiols such as glutathione (GSH) and surface-exposed Cys in the intracellular redox buffering system.

To achieve the environmental sensitivity, our strategy involved replacing the TPE unit with a push-pull AIE fluorophore (Figure 1A). Push-pull dyes with both electron donor and acceptor experience excited-state charge transfer, which is stabilized by interaction with the dipoles of solvent and resulting in emission red-shift in more polar solvents.[13] Being sensitive to polarity, push-pull dyes have been extensively used to study the biophysical properties of lipid membranes and for the detection of biomolecular interactions such as protein-lipid interaction.[14] On the other hand, the activation of AIE dyes through restriction of intramolecular motions has been used in designing AIE probes for protein detection and characterization.[15] To construct a push-pull AIE fluorophore while retaining a similar molecular structure, we changed one of the phenyl rings of TPE to an electron-withdrawing cyano group (Figure 1A).[16] Methoxy and dimethylamino substituents are used as electron donors, which also improve the compatibility of the dyes in aqueous media.[13]

Dye Synthesis and Photophysical Characterization

The synthetic routes to compound **2**-**4** are shown in Scheme S1 in the supporting information. In short, a Knoevenagel condensation reaction between respective diarylketones and bromobenzyl cyanide gave the donor-acceptor cores of interest. A copper catalyzed amination of aryl-bromide cores led to amine analogs that were further converted to maleimide in the final products using maleic anhydride. The final products **2**-**4** were characterized by ^{1}H, ^{13}C NMR, high-resolution mass spectrometry, and FT-IR spectroscopy (refer to SI). The structures were further confirmed by single crystal X-ray crystallography (Figure S42 and Table S3 – S5). The core of triphenylacrylonitrile (TPAN) adopts a highly twisted geometry with the torsion angles ranging from 121.61 – 146.74° between the phenyl rings and the central double bond (Figure S43). Such geometry reduces aggregation-caused quenching from strong π-π stacking (Figure S44-46).[15,17] Comparison of the UV-Vis absorption spectra of dyes revealed the effect of the electron donating groups on the π conjugate system of TPAN (Figure 1C). There are red-shifts in the absorption maximum from **2** (318 nm) to methoxy-substituted **3** (350 nm) and dimethylamino-substituted **4** (393 nm). With the largest red-shift and strongest donor-acceptor effect, dye **4** (NTPAN-MI) was selected for subsequent studies.

NTPAN-MI is inherently non-fluorescent until it reacts with a thiol via the C=C on the MI.[18] This observation was supported by DFT calculations showing a low-lying nπ* state between HOMO and LUMO of NTPAN induced by the MI group (Figure 1B). This energy level that contributed to the non-radiative decay of excited NTPAN-MI was not present in the saturated succinimide analog which was formed after thiol conjugation to the MI (Figure S1). In addition, we observed that electron density for HOMO levels were more localized around the electron-donating groups while the LUMO were closer to the electron-withdrawing cyano group (Figure 1B). Such electron distribution is characteristic of push-pull dyes with photoinduced

charge transfer, which results in the solvatochromism in their fluorescence.[13] In order to study the

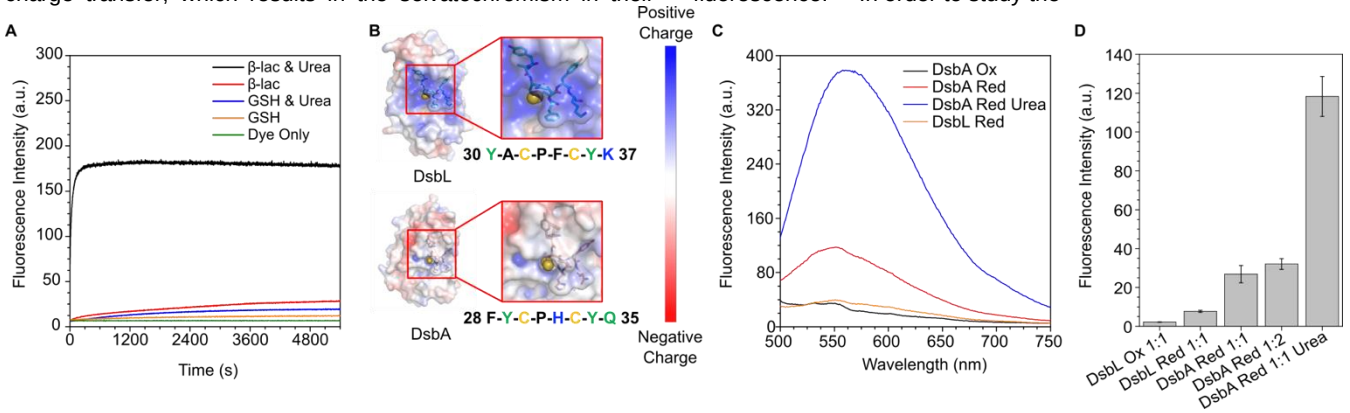

Figure 2. *In vitro* fluorescence studies with model proteins. (A) Fluorescence kinetic traces of NTPAN-MI with folded/unfolded β-lac and GSH. Denaturant: 6 M urea in PBS; protein concentration: 250 μM; dye concentration: 50 μM. Excitation: 405 nm; emission: 540 nm. (B) Crystal structures of DsbA and DsbL, adapted from Ref 19. The red box highlights the position of the surface-exposed Cys on the proteins. (C) Emission spectra of NTPAN-MI with oxidized (Ox) or reduced (Red) forms of DsbA and DsbL in folded/unfolded (Urea) status. Sample preparation showed in SI. (D) Endpoint intensity of NTPAN-MI fluorescence with folded oxidized/reduced DsbL, folded reduced DsbA in 1:1 or 1:2 protein-to-dye molar ratio, or with unfolded reduced DsbA. Data extracted from kinetic traces shown in Figure S7B. Protein concentration: 25 μM; dye concentration: 25 or 50 μM; excitation and emission filter: 390/20 and 540/50 nm respectively. n =3 biological replicates; mean ± s.d.

fluorescence behavior, the thiol-bound form of NTPAN-MI (**4a**) was prepared (Figure 1D and Scheme S1). The UV-Vis absorption spectra of **4a** exhibited negligible shift among solvents with different polarity (Figure S2-3). The emission spectra (excitation at 405 nm), on the other hand, displayed a large red-shift with the increase of solvent polarity. The emission peak shifted from 463 nm in nonpolar toluene to 586 nm in phosphate buffered saline (PBS) solution (Figure 1E). The correlation between the emission maximum and the dielectric constant of the solvent is in a linear relationship (Figure 1F). The nature of the absorbance and emission profiles of the thiol-bound NTPAN-MI would allow us to estimate and report on the local environment of bound unfolded proteins in a cell.

Surface Exposed vs. Buried Cys on Dye Reactivity

To validate this hypothesis, the reactivity of NTPAN-MI was first tested *in vitro* with model proteins. β-lactoglobulin (β-lac) with 5 buried Cys in the thiol form was chosen as a test protein. NTPAN-MI showed weak fluorescence in the presence of folded β-lac but became highly emissive when β-lac was unfolded in 6 M urea (Figure 2A). The kinetics curve indicated NTPAN-MI is able to react with exposed Cys rapidly when β-lac unfolds. Addition of thiol-blocking reagents, such as *N*-methylmaleimide (NMM), reduced NTPAN-MI emission intensity effectively, especially with unfolded proteins, indicating they are competing for the same species, i.e. Cys on the proteins (Figure S4). Replacing Cys-reactive MI to an inert Br substituent yielded a control probe, NTPAN-Br, which exhibited high background fluorescence in aqueous solution (Figure S5). No fluorescence changes could be observed between folded and unfolded proteins, further confirming the importance of the MI moiety in the detection process. On the other hand, the presence of hydrophilic GSH, even in much higher concentration, could not induce NTPAN fluorescence to the same extent as the unfolded β-lac (Figure S6). These results suggest that the reactivity of NTPAN-MI with hydrophilic GSH is much lower than that with thiol containing unfolded protein, and there was minimal self-aggregation of the GSH-bound NTPAN-MI.

Next, the role of hydrophobic surface in NTPAN-MI reactivity was investigated with two thiol disulfide oxidoreductases (Dsb) which contain a surface-exposed Cys residue in distinct environments. DsbA and DsbL proteins share a very similar three-dimensional structure encompassing two cysteines, one buried and one surface exposed, that could be oxidized to disulfide bonded or reduced to two free thiols.[19] A major difference between these proteins is the local environment surrounding the surface exposed cysteine: DsbA is hydrophobic and DsbL, hydrophilic (Figure 2B).[19] We first tested the Dsb proteins in their oxidized disulfide bonded form, which, as expected, could not activate the NTPAN-MI fluorescence (Figure 2C). Incubation of NTPAN-MI with reduced Dsb proteins, yielded approximately 25-fold fluorescence enhancement on DsbA but minimal enhancement on DsbL, indicating the interaction between NTPAN-MI and Cys is more favored in a hydrophobic environment. When protein-to-dye molar ratios were changed from 1:1 to 1:2, the fluorescence intensity remained comparable, implying that NTPAN-MI does not perturb the folded structure of the proteins or access the buried Cys residue (Figure 2D). The conjugation of one NTPAN-MI molecule with folded DsbA was further confirmed by intact protein mass spectrometry (Figure S7). This fluorescence intensity for the hydrophobic DsbA, however, was negligible compared to the significant 120-fold increase in intensity for reduced DsbA in the unfolded state (25 fold). This suggests that when reacted with surface-exposed Cys, the dye molecule is not fully restricted and the fluorescence remains relatively weak, when compared to the substantial fluorescence emission of unfolded DsbA conjugated NTPAN-MI.

Cys reactivity is dependent on pH.[20] To test the influence of pH on NTPAN-MI reactivity, we measured the fluorescence at the physiological pH range (~4–8) (Figure S8-S9). Minimal

change in fluorescence intensity was observed in the presence of folded reduced DsbA with NTPAN-MI between pH 4.27-7.10 with a slight

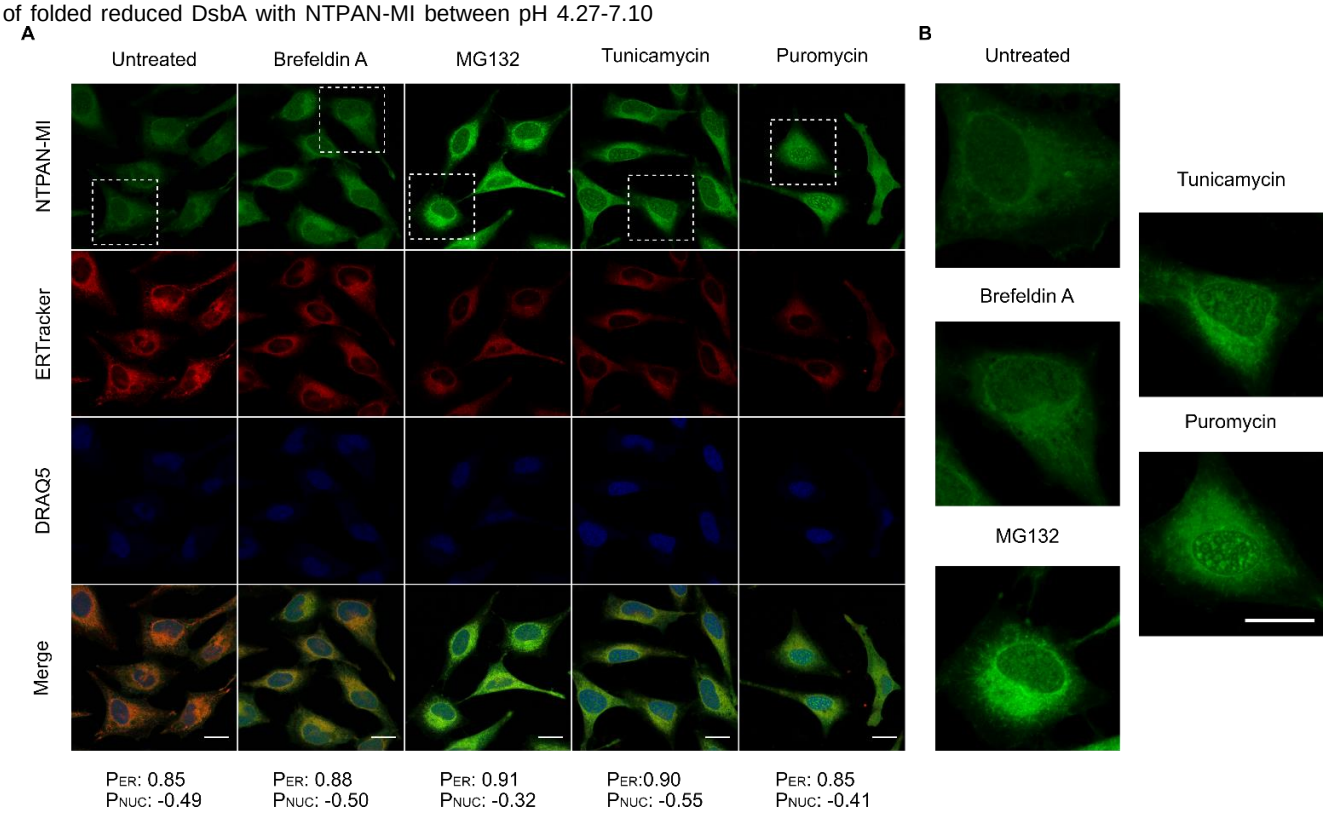

Figure 3. Intracellular distribution of unfolded proteins revealed by NTPAN-MI. (A) Confocal images of control and stressed HeLa cells stained with NTPAN-MI with ER-Tracker™ Red and DRAQ5™ counterstain to view colocalization with endoplasmic reticulum (ER) and nucleus respectively. P_{ER} and P_{NUC} are the calculated Pearson correlation values for NTPAN-MI in ER and nucleus respectively. Scale bar: 20 µm. (B) Enlarged images of insets in panel A. Scale bar 20µm.

increase at pH 7.89 (Figure S9A). Normalized fluorescence kinetic traces did not show any significant deviation between the varying pH, implying that the reactivity of NTPAN-MI with Cys is less likely to be influenced by pH variation within the physiological range (Figure S9B).

Visualizing Unfolded Proteins in Cytoplasm and Nucleus

The *in-vitro* experiments with model proteins confirmed that the major fluorescence enhancement of NTPAN-MI could be attributed to the reaction with unfolded proteins containing non-disulfide bonded Cys residues. Next, the behavior of NTPAN-MI in cells was examined. Cytotoxicity assay showed that NTPAN-MI posed no significant toxicity towards cells at concentration up to 100 µM and incubation time as long as 12 h (Figure S10). Confocal imaging revealed that NTPAN-MI was readily permeable to not only the plasma membrane but also the nuclear membrane after 30 min of staining (Figure 3). To examine the intracellular distribution of NTPAN-MI (pseudo green), the cells were counterstained with ER-Tracker™ Red (pseudo red) and DRAQ5™ (pseudo blue) to localize the ER and nucleus respectively. The settings of the three channels were optimized to avoid signal bleed-through (Figure S11)

In control/untreated cells, NTPAN-MI displayed dim fluorescence signals homogeneously distributed in the cells (Figure 3). The ability of NTPAN-MI to detect potentially unfolded proteins *in cellulo* was assessed using the drugs that induce proteostasis stress. Puromycin, tunicamycin, brefeldin A, and MG132, which interfere with the protein synthesis, folding, transport and degradation pathways, respectively, were chosen in the study.[21-24] Disruption of any of these pathways could lead to the backlog of premature or unfolded proteins accumulated in the cells, which was confirmed by the significant increase of NTPAN-MI fluorescence of prelabeled cell protein lysates (Figure S12). The fluorescence was normalized to total protein concentration under each condition to avoid the variation of protein concentration caused by the stressors. The fluorescence enhancement in stressed cells could also be seen from confocal images (Figure 3). The NTPAN-MI staining patterns in the cytoplasm were highly colocalized with ER-Tracker™ Red, with the Pearson correlation factor (P_{ER}) between 0.85-0.91 under all conditions. Despite of penetration of NTPAN-MI into the nucleus, we obtained negative correlation values (P_{NUC}) with the DNA stain DRAQ5™, suggesting that proteins rather than DNA were being labelled by the dye. Distinct protein condensates with bright NTPAN-MI fluorescence were observed in the nucleus under certain stress conditions (Figure 3B), in particular, puromycin treatment, indicating the unfolded protein load also increased in the nucleus in response to such proteostasis stress.

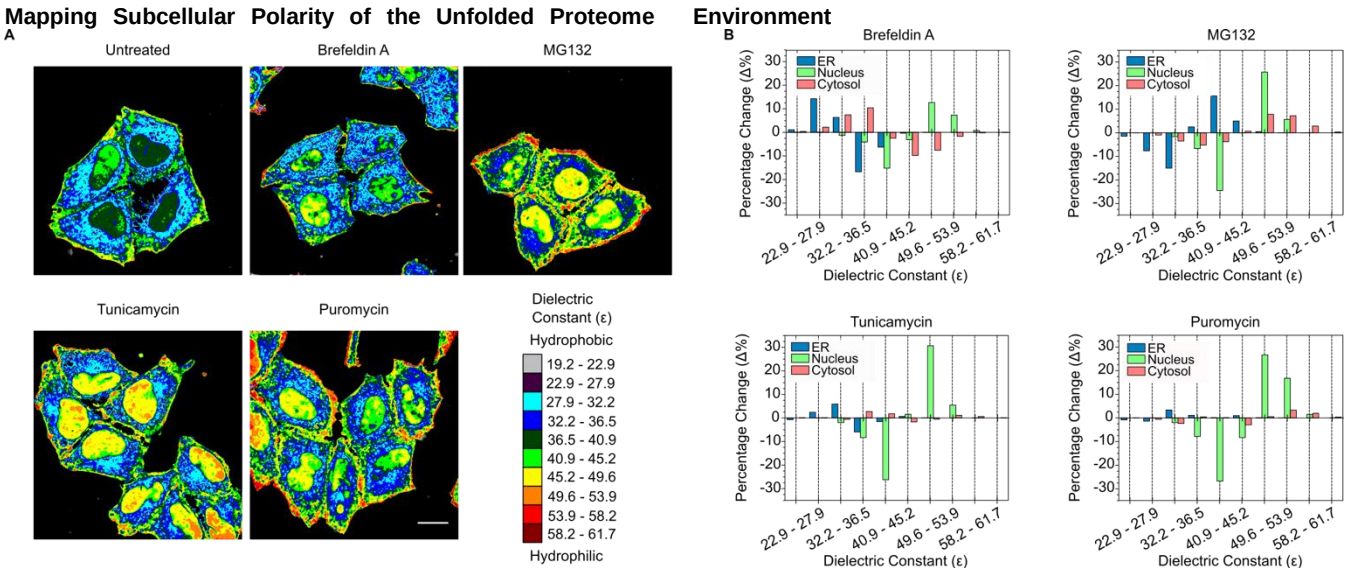

Figure 4. Mapping and quantifying intracellular polarity of unfolded protein environment. (A) Representative images of intracellular dielectric constant (ε) distribution in untreated and stressed cells stained by NTPAN-MI resolved from spectral phasor analysis. Excitation: 405 nm; emission: acquired from 415-700 nm with 8.9 nm bin widths to obtain 32 channels. Scale bar: 20 μm. (B) Changes in ε distributions of unfolded protein environment in ER, nucleus and cytosol in brefeldin A, MG132, tunicamycin, and puromycin treated cells compared to untreated cells. A positive or negative change in the plots reflects a respective increase or decrease in the pixel population within that specific ε range. The analysis is based on 10 images with total 38-56 cells analyzed in each condition.

Following the characterization of dye distribution in cells, we took advantage of the solvatochromism of NTPAN-MI (*cf.* Figure 1E, Figure S3) to assess the local polarity of the bound proteins in cells. Spectral phasor analysis is a powerful method that allows us to deconvolute and identify the emission spectra of pixels on a global scale in an acquired image.[25,26] Upon excited by 405 nm laser, confocal images were collected in every 8.9 nm from 415 to 700 nm in 32 channels (Figure S13). We then focused on using the phasor angle to determine emission spectral wavelength from the 32 channel images to estimate the dielectric constant (ε) of individual pixels. By using spectral phasor analysis, we found the ε values varied in different compartments of the cells. The labeled unfolded proteins experienced ε in a range of 22-32 in the ER, 32-36 at the interface of ER and cytoplasm, 36-45 inside the nucleus, and 45-50 on the plasma membrane in the control/untreated cells. These values are generally consistent with the dielectric constant in cytoplasm and nucleus measured by electrochemical methods.[27,28]

The above results demonstrated that the unfolded proteins in the ER are mostly in a hydrophobic environment with low ε while in the nucleus the environment is more hydrophilic. Charged species are most likely to contribute to the dielectric properties of the intracellular environment.[28] The distinct ε observed in the nucleus could be attributed to the environment rich in highly charged nucleic acids. The interaction of the unfolded proteins with nucleic acids creates an environment with dielectric property differing from either non-charged protein-rich (lower ε) or aqueous environment (higher ε). This hypothesis is also supported by the previous reported ε value of stress granules, composed of proteins and RNAs, sitting in the range of acetonitrile and DMSO (ε = 40-50).[9,28] As a control experiment, permeating the cell membrane with Triton X-100 resulted in a highly polar environment in all cell compartments (Figure S14). Upon the addition of the stressors puromycin, tunicamycin, brefeldin A and MG132, the overall intracellular environment became even more discrete (Figure 4A). Although each stressor led to a distinct pattern of ε distribution, the common feature was that the unfolded protein environment in the nucleus became much more hydrophilic (ε shifting to 45-54).

To further quantify the intracellular ε distribution in a larger population of cells, we separated NTPAN-MI signals into three groups based on subcellular locations and fluorescence intensity, namely the ER, nucleus and cytosol (Figure S15). 10 images with total 38-56 cells in each condition were acquired for the spectral phasor analysis. The same spectral gating strategy was applied to the estimation and subsequent quantification of environmental polarity in individual cellular compartments in all acquired images (Figure S15, Table S2). Figure 4B shows the comparison of the population of pixels at a specific dielectric constant range of the stressed cells when compared to those in control cells. A positive or negative change in the plots reflects a respective increase or decrease in the pixel population within that specific polarity range. A positive shift to lower ε region was found in the ER when the cells were treated with ER stressors such as brefeldin A and tunicamycin (Figure 4B). Brefeldin A blocks protein transport from ER to Golgi, while tunicamycin inhibits the *N*-linked glycosylation of proteins in ER.[21,22] Both lead to the build-up of misfolded proteins in the ER, possibly with increased hydrophobic patches exposed, resulting in a more hydrophobic environment for NTPAN-MI. MG132, a proteasome inhibitor, causes a backlog of ubiquitylated proteins that would normally be degraded in the cells.[24] Spectral profile of NTPAN-MI reflected that these proteins in both ER and cytosol were in a

more hydrophilic environment upon MG132 treatment. This was in line with previously reported observation that ubiquitylated proteins in MG132-treated cells were more soluble in PBS, indicating that these proteins were more likely to reside in polar environments.[29] Puromycin, a protein synthesis inhibitor, did not induce noticeable change in the unfolded protein environment in the cytoplasm. However, across all stress treatments, the nucleus had a large shift in the population of pixels in the more hydrophilic, higher ε region. Such changes could arise from the impairment of nucleocytoplasmic transport pathways under stress.[30,31] Recent literature also pointed out the interaction of unfolded proteins and RNA in the nucleus as a strategy to temporarily store the dynamic unfolded proteins and prevent the formation of irreversible protein aggregates.[32] This is an exciting observation with further experiments currently being carried out.

Measuring Proteostasis Collapse in Influenza Virus Infected Cells

With the encouraging results in drug-induced stress models, NTPAN-MI was further applied to assess proteostasis stress induced by virus infection. Cells with successful influenza A virus (IAV) infection were recognized by the immunostaining of IAV nucleoproteins (NP). Flow cytometry analysis revealed a significant increase in NTPAN-MI fluorescence in the infected (IAV+) group, in comparison to the uninfected (IAV-) group, in both suspension P815 and adherent A549 cell-lines (Figure 5A,B; Figure S16). Confocal imaging showed that the NTPAN-MI staining pattern changed from homogenous distribution in uninfected cells to discrete puncta in IAV-infected cells (Figure 5C). A similar phenomenon has been observed on the autophagosome marker LC3 protein upon lipidation in cells with IAV infection.[33] Interestingly, little colocalization was observed of NTPAN-MI fluorescence with NP immunofluorescence, possibly due to the Cys residues being buried in NP [Figure 5C, S17B (Z-stack)].[34] The IAV virus hijacks the host proteostasis machinery to facilitate the synthesis and processing of viral proteins for their own replication.[35] Our results showed that such process disrupts the protein quality control of the host cells, as revealed by the increase of NTPAN-MI fluorescence. Spectral phasor analysis, however, was not applied to this particular case due to the requirements of cell permeabilization for NP immunostaining (*cf.* Figure S14).

Conclusion

In summary, a simple approach to quantifying the change of intracellular polarity accompanying protein misfolding was presented. NTPAN-MI fluorescence can report on the unfolded protein load not only in the cytoplasm but, for the first time, in the nucleus. Spectral phasor analysis of protein-bound NTPAN-MI solvatochromism reveals the crosstalk between the nuclear and cytoplasmic protein quality control, an area still underexplored. Our method provides possibilities to investigate the role of subcellular polarity in driving fundamental biological processes involved in protein quality control and stress response. This method would find many applications including in understanding the pathogenesis, finding biomarkers and screening drugs that rectify proteostasis for the treatment of neurodegenerative diseases.

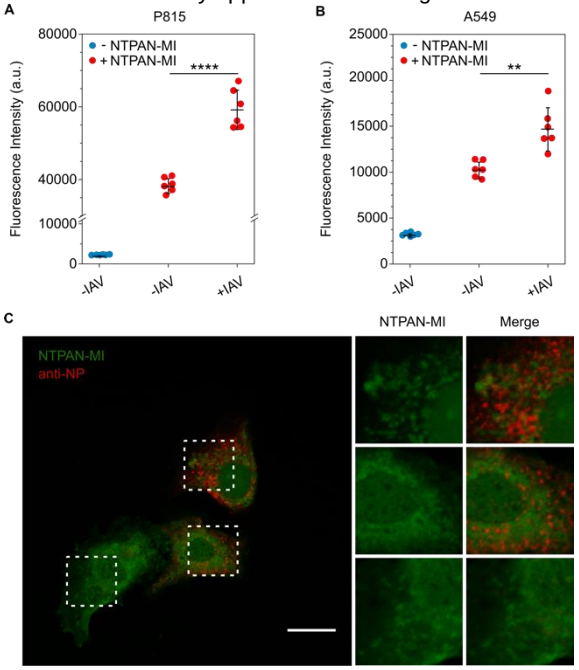

Figure 5. NTPAN-MI reveals proteostasis collapse in influenza virus infected cells. (A) P815 and (B) A549 cells were mock-infected or infected with IAV (PR8 (H1N1)) at MOI=5 for overnight. Cells were then stained with NTPAN-MI (50 μM) for 30 min and analysed by flow cytometry. Two independent experiments were conducted with similar results, and each independent experiment included 3 biological replicates; mean ± s.d. **P < 0.01; ****P < 0.0001. (C) Confocal images of NTPAN-MI stained A549 cells with anti-IAV NP counterstain. Scale bar: 20 μm.

Acknowledgements

We thank Dr Peter Lock and LIMS Bioimaging Platform, La Trobe University for the technical support and access to the confocal microscope and flow cytometer. We thank Dr Swati Varshney, A/Prof Nicholas A. Williamson and Bio21 Mass Spectrometry and Proteomics Facility for technical support and access to mass spectrometers. This work was supported by grants to Y.H. (Australian Research Council DE170100058, Rebecca L. Cooper Medical Research Foundation PG2018043, National Health and Medical Research Council GNT1161803 and Australia-China Science and Research Fund-Joint Research Centre on Personal Health Technologies), WWHW (Australian Research Council CE17100026) and JMW (Australian Synchrotron for beamtime via the Collaborative Access Program Project Number 13618b).

Keywords: Fluorescent probes • solvatochromism • aggregation-induced emission • unfolded protein • proteostasis

[1] C. M. Dobson, *Semin. Cell Dev. Biol.* **2004,** *15*, 3-16.
[2] R. I. Morimoto, *Genes Dev.* **2008,** *22*, 1427-1438.
[3] F. U. Hartl, A. Bracher, M. Hayer-Hartl, *Nature*, **2011**, 475, 324-332.

[4] E. T. Powers, R. I. Morimoto; A. Dillin, J. W. Kelly, W. E. Balch, *Annu. Rev. Biochem.* **2009,** *78*, 959-991.
[5] B. Wolozin, *Mol. Neurodegener.* **2012,** *7*, 56.
[6] S. Alberti, S. Carra, *J. Mol. Biol.* **2018,** *430*, 4711-4729.
[7] S. F. Banani, H. O. Lee, A. A. Hyman, M. K. Rosen, *Nat. Rev. Mol. Cell Biol.* **2017**, *18*, 285-298.
[8] T. J. Nott, E. Petsalaki, P. Farber, D. Jervis, E. Fussner, A. Plochowietz, T. D. Craggs, D. P. Bazett-Jones, T. Pawson, J. D. Forman-Kay, A. J. Baldwin, *Molecular Cell* **2015,** *57*, 936-947.
[9] T. J. Nott, T. D. Craggs, A. J. Baldwin, *Nat. Chem.* **2016,** *8*, 570-576.
[10] a) Y. Liu, K. Miao, Y. Li, M. Fares, S. Chen, X. Zhang, *Biochemistry* **2018,** *57*, 4663-4674. b) M. Fares, Y. Li, Y. Liu, K. Miao, Z. Gao, Y. Zhai, X. Zhang, *Bioconjugate Chem.* **2018**, *29*, 215-224.
[11] J. Tyedmers, A. Mogk, B. Bukau, *Nat. Rev. Mol. Cell Biol.* **2010**, *11*, 777-788.
[12] M. Z. Chen, N. S. Moily, J. L. Bridgford, R. J. Wood, M. Radwan, T. A. Smith, Z. Song, B. Z. Tang, L. Tilley, X. Xu, G. E. Reid, M. A. Pouladi, Y. Hong, D. M. Hatters, *Nat. Commun.* **2017,** *8*, 474.
[13] S. Zhang, M. Liu, L. Y. F. Tan, Q. Hong, Z. L. Pow, T. C. Owyong, S. Ding, W. W. H. Wong, Y. Hong, *Chem. Asian J.* **2019,** *14*, 904-909.
[14] a) A. S. Klymchenko, *Acc. Chem. Res.* **2017**, *50*, 366-375; b) Y. Hong, J. Muenzner, S. K. Grimm, E. V. Pletneva, *J. Am. Chem. Soc.* **2012,** *134*, 18713-18723.
[15] a) S. Xie, A. Y. H. Wong, S. Chen, B. Z. Tang, *Chem. Eur. J.* **2019**, *25*, 5824-5847; b) K. C. Chong, F. Hu, B. Liu, *Mater. Chem. Front.* **2019**, *3*, 12-24; c) H. GAO, X. ZHANG, C. Chen, K. Li, D. Ding, *Adv. Biosyst.* **2018**, *2*, p1800074; d) S. Ding, M. Liu, Y. Hong, *Sci. China Chem*. **2018**, *61*, 882-891; e) J. Xiong, X. Z. Cao, S. Q. Yang, Z. H. Mo, W. Wang, W. B. Zeng, *Protein Pept. Lett.* **2018**, *25*, 548-559; f) J. Mei, N. L. C. Leung, R. T. K. Kwok, J. W. Y. Lam, B. Z. Tang *Chem. Rev.* **2015**, *115*, 11718-11940.
[16] Y. Gong, Y. Tan, J. Liu, P. Lu, C. Feng, W. Z. Yuan, Y. Lu, J. Z. Sun, G. He, Y. Zhang, *Chem. Commun.* **2013**, *49*, 4009-4011.
[17] Y. Cai, L. Du, K. Samedov, X. Gu, F. Qi, H. H. Y. Sung, B. O. Patrick, Z. Yan, X. Jiang, H. Zhang, J. W. Y. Lam, I. D. Williams, D. L. Phillips, A. Qin, B. Z. Tang, *Chem. Sci.* **2018,** *9*, 4662-4670.
[18] K. Caron, V. Lachapelle, J. W. Keillor, *Org. Biomol. Chem.* **2011**, *9*, 185-197.
[19] B. Heras, M. Totsika, R. Jarrott, S. R. Shouldice, G. Guncar, M. E. Achard, T. J. Wells, M. P. Argente, A. G. McEwan, M. A. Schembri, *J. Biol. Chem.* **2010,** *285*, 18423-18432.
[20] R. A. Bednar, *Biochemistry* **1990,** *29*, 3684-3690.
[21] W. C. Mahoney, D. Duksin, *J. Biol. Chem.* **1979,** *254*, 6572-6576.
[22] J. Lippincott-Schwartz, L. C. Yuan, B.-J. S. Cell, *Cell* **1989,** *55*, 801-813.
[23] M. B. Yarmolinsky, G. L. Delahaba, *P. Natl. Acad. Sci. USA* **1959,** *45*, 1721-1729.
[24] D. H. Lee, A. L. Goldberg, *Trends Cell Biol.* **1998,** *8*, 397-403.
[25] O. Golfetto, E. Hinde, E. Gratton, The Laurdan Spectral Phasor Method to Explore Membrane Micro-heterogeneity and Lipid Domains in Live Cells In *Methods in Membrane Lipids* (Ed: D. M. Owen) Springer New York: New York, NY, **2015**; pp 273-290.
[26] F. Fereidouni, A. N. Bader, H. C. Gerritsen, *Opt. Express* **2012,** *20*, 12729-12741.
[27] W. Wang, K. Foley, X. Shan, S. Wang, S. Eaton, V. J. Nagaraj, P. Wiktor, U. Patel, N. Tao, *Nat. Chem.* **2011,** *3*, 249.
[28] F.-X. Theillet, A. Binolfi, T. Frembgen-Kesner, K. Hingorani, M. Sarkar, C. Kyne, C. Li, P. B. Crowley, L. Gierasch, G. J. Pielak, A. H. Elcock, A. Gershenson, P. Selenko, *Chem. Rev.* **2014,** *114*, 6661-6714.
[29] G. Xu, A. Pattamatta, R. Hildago, M. C. Pace, H. Brown, D. R. Borchelt, *J. Cell Sci.* **2016,** *129*, 1892-1901.
[30] A. C. Woerner, F. Frottin, D. Hornburg, L. R. Feng, F. Meissner, M. Patra, J. Tatzelt, M. Mann, K. F. Winklhofer, F. U. Hartl, M. S. Hipp, *Science* **2016,** *351*, 173.
[31] X. Sui, D. E. V. Pires, S. Nie, G. Vecchi, M. Vendruscolo, D. B. Ascher, G. E. Reid, D. M. Hatters, *bioRxiv* **2019**, 692103.
[32] F. Frottin, F. Schueder, S. Tiwary, T. R. Gupta, R. Korner, T. Schlichthaerle, J. Cox, R. Jungmann, F. U. Hartl, *Science*, **2019**, *365*, 342-247.
[33] Z. Zhou, X. Jiang, D. Liu, Z. Fan, X. Hu, J. Yan, M. Wang, G. F. Gao, *Autophagy* **2009,** *5*, 321-328.
[34] Q. Ye, R. M. Krug, Y. J. Tao, *Nature* **2006,** *444*, 1078-1082.
[35] M. Marques, B. Ramos, A. R. Soares, D. Ribeiro, *Cells* **2019,** *8*, 228.

Entry for the Table of Contents

RESEARCH ARTICLE

Here we report a strategy based on a multi-responsive probe, in combination with spectral phasor analysis, to monitor the change of subcellular polarity in response to protein unfolding.

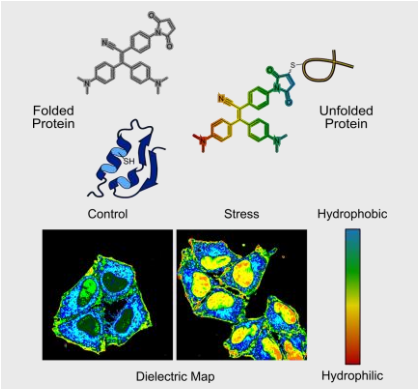

Tze Cin Owyong, Pramod Subedi, Jieru Deng, Elizabeth Hinde, Jason J. Paxman, Jonathan M. White, Weisan Chen, Begoña Heras, Wallace W. H. Wong, Yuning Hong**

Page No. – Page No.

A Molecular Chameleon for Mapping Subcellular Polarity of Unfolded Proteome Environment